Preface

In the booming fields of the life and material sciences, advances are taking place on all fronts and often involve the use of luminescence techniques as analytical tools and detection methods due to their high sensitivity, intrinsic selectivity, noninvasive (or at least minimally invasive) character, comparative ease of use, potential for multiplexing applications, and remote accessibility of signals. Despite the fact that the measurement of fluorescence—with its birth marked by the study of Sir Stokes on quinine sulfate in 1852—is not a new technique and many fluorescence techniques have matured to a state where quantification is desired, standardization of the broad variety of fluorescence methods and applications is still in its infancy as compared to other prominent (bio)analytical methods.

It is still often overlooked that all types of fluorescence measurements yield signals containing both analyte-specific and instrument-specific contributions. Furthermore, the absorption and fluorescence of most fluorophores is sensitive to their microenvironment, and this can hamper quantification based on measurements of relative fluorescence intensities as well as accurate measurements of absolute fluorescence intensities. Hence, the realization of a truly quantitative measurement is inherently challenging. This situation renders quality assurance in fluorometry very important, especially with respect to the increasing complexity of instrumentation, and the blackbox-type of present-day instruments and software. This may compromise future applications of fluorescence techniques in strongly regulated areas like medical diagnostics and clinical chemistry that are within reach.

As a result, there is an ever increasing need for (a) recommendations and guidelines for the characterization and performance validation of fluorescence instrumentation and the performance of typical fluorescence measurements, and (b) for an improved understanding of fluorescence-inherent sources of error. This is closely linked to the availability of suitable and easily handled standards that can be operated under routine analytical conditions, are adequately characterized, and meet overall accepted quality criteria.

Within this context, the aim of this book is to provide a unique overview on the current state of instrumentation and application of a very broad variety of fluorescence techniques employed in the material and especially in the life sciences thereby highlighting the present state of quality assurance and the need

for future standards. Methods included span microfluorometric techniques used for immunoassays, fluorescence microscopic and imaging techniques including single molecule spectroscopy, flow cytometry and fluorescence in situ hybridization to the microarray technology and technologies used in biomedical diagnostics like in vivo fluorescence imaging. Method-inherent advantages, limitations, and sources of uncertainties are addressed, often within the context of typical and upcoming applications. The ultimate goal is to make users of fluorescence techniques more aware of necessary steps to improve the overall reliability and comparability of fluorescence data to encourage the further broadening of fluorescence applications.

I wish to express my appreciation and special thanks to the individuals who insisted and encouraged me in the preparation of this book. These include Dr. K. Hoffmann, Dr. R. Nitschke, Dr. L. Wang, Dr. R. Zucker, and especially Prof. Dr. O. Wolfbeis for help with the choice of authors and reviewers. And finally, Jürgen and Claudia, for their continuous support and encouragement.

Berlin, July 2008   Dr. Ute Resch-Genger

Characterization and Calibration in Wide Field and Sectioned Fluorescence Microscopy SIPcharts

Fred Brakenhoff (✉) · Jurriaan Zwier

Swammerdam Institute for Life Sciences, University of Amsterdam, Kruislaan 316,
1098 SM Amsterdam, The Netherlands
brakenho@science.uva.nl

Abstract A fluorescence image calibration method is introduced based on the use of standardized uniformly fluorescing reference layers. Crucial to the approach is that these layers are highly uniform. It is demonstrated to be effective for the correction of non-uniform imaging characteristics across the image (shading correction) as well as for relating fluorescence intensities between images taken with different microscopes or imaging conditions. The approach can be used both in wide field or regular and sectioned (see the section on fluorescence microscopy).

In wide field it is shown that in addition the variation of the illumination intensity over the image can be determined on the basis of the uniform bleaching characteristics of the layers. This permits correction for the latter and makes bleach-rate-related imaging in wide field microscopy practical.

The significant potential of these layers for calibration in quantitative fluorescence microscopy is illustrated with a series of applications. The approach is also shown to be valuable for general microscope testing and characterization. Specifically in sectioning, specifically confocal, microscopy a set of parameters derived from through-focus datasets of such layers can be used to define a number of properties relevant to sectioned imaging. The main characteristics of a particular imaging situation can then be summarized in a sectioned imaging property chart (SIPchart), which turns out to be a very useful tool for characterizing the properties of particular sectioned imaging systems.

Abbreviations

$D(x,y)$	Detection efficiency distribution
DPPC	Dipalmitoylphosphatidylcholine
$F(x,y)$	Fluorescer distribution
FRAP	Fluorescence Recovery after Photobleaching
FRET	Fluorescence Resonance Energy Transfer
$I(x,y)$	Illumination distribution
$k(x,y)$	Bleach rate distribution
LC	Liquid condensed
LE	Liquid expanded
NA	Numerical Aperture
NBDPC	NBD-phosphatidylcholine
$P(x,y)$	Product distribution
PSF	Point Spread Function
SIPchart	Sectioned Imaging Property chart
t_i (s)	Exposure time

1
Introduction

A fluorescence image calibration method is introduced based on the use of standardized uniformly fluorescing reference layers. Crucial to the approach is that these layers are highly uniform. It is demonstrated to be effective for the correction of non-uniform imaging characteristics across the image (shading correction) as well as for relating fluorescence intensities between images taken with different microscopes or imaging conditions. The approach can be used both in wide field or regular (Sect. 2) and sectioned (Sect. 3) fluorescence microscopy.

In wide field it is shown that in addition the variation of the illumination intensity over the image can be determined on the basis of the uniform bleaching characteristics of the layers. This permits correction for

the latter and makes bleach-rate-related imaging in wide field microscopy practical.

The significant potential of these layers for calibration in quantitative fluorescence microscopy is illustrated with a series of applications. The approach is also shown to be valuable for general microscope testing and characterization.

Specifically, in sectioning microscopy, a set of parameters derived from through-focus datasets of such layers can be used to define a number of properties relevant to sectioned imaging. The main characteristics of a particular imaging situation can then be summarized in a sectioned imaging property chart, or SIPchart, which turns out to be a very useful tool for characterizing the properties of particular sectioned imaging systems.

2
Image Calibration in Wide Field Fluorescence Microscopy

2.1
Introducing Calibration in Wide Field Microscopy

For the purpose of this section on wide field imaging characterization the pixellated image P(x,y) – also called in this chapter the product distribution – of a fluorescence microscope can be described as:

$$P(x,y) = I(x,y) \cdot D(x,y) \cdot F(x,y) \cdot t_i(s) , \qquad (1)$$

where $I(x,y)$ is the illumination distribution over the image field of view, $D(x,y)$ the detection efficiency distribution, $F(x,y)$ the fluorescence distribution from pixel to pixel over the specimen, t_i (s) the image exposure time in seconds s, and x,y the image pixel coordinates.

In this section we address two types of fluorescence calibration:

1. Fluorescence of the fluorescence image intensity. This involves calibration at the level of the product $I(x,y) \cdot D(x,y)$ as needed for shading correction and image comparison.
2. Fluorescence of the variations in illumination intensity $I(x,y)$ as required for the correction in bleach rate imaging.

The key to the approach is the use of fluorescent reference layers for the calibration that are both to a high degree *spatially uniform* as well as *reproducible*. In the presented procedure the fluorescence image is calibrated with the help of an image of the reference layer taken under identical imaging conditions as the image to be calibrated.

The work is partly a continuation of earlier work of our group [1, 2] and is related to the work done by Castleman [3] and Jericevic et al. [4]. The latter already showed that with a calibration layer spatial variation of the product of the

illumination and detection pathways could be corrected. Ghauharali et al. [1] did obtain in addition separate illumination distributions by using a mono-exponential function for fitting the observed bleaching of their test layers. Fitting the bleaching characteristics using stretched exponential decay kinetics provides much better fits then with a mono-exponential function dependence.

Originally, we intended to develop two types of reference layers: one uniformly fluorescing, but non-bleaching for calibrating the product distribution P(x,y), and one uniformly bleaching to determine the illumination distribution. However, it turned out that the latter layers as developed could serve effectively both functions combined. While the bleaching was sufficiently slow to permit for fluorescence calibration with the first or second image of such a layer, it still showed enough bleaching over a finite time span to be practical for determining the illumination distribution from the bleaching dependence.

After illustrating the necessity for using stretched exponential fitting, we show that the fluorescence reference layers are suitable for the determination of both I(x,y) and D(x,y) in a range of intensities relevant to regular wide-field fluorescence microscopes. Subsequently, it is shown that the reference layers can be manufactured with narrow tolerances and with fluorescence and bleaching characteristics uniform within a few percent.

2.2
Bleach Kinetics

The excitation illumination distribution in a microscope image can be determined from the bleach behavior at each pixel point in a series of images taken as a function of exposure time. Ghauharali et al. [1, 2] have shown that with a suitable photo-bleachable test layer the distribution of both the excitation intensity and the detection efficiency over the image can be determined by this approach. Following up on their findings we set out to develop optimized calibration or reference layers which should show ideally mono-exponential irreversible photo-bleach kinetics with respect to the total irradiation dose of incident light. In practice, we found that none of the layers we produced did satisfy this requirement. Even at low dye concentrations where dye-dye interactions are minimized, still no mono-exponential decay could be observed in the layers produced by us. This does not come as a surprise, as it is known [5, 6] from polymer kinetics that in polymer films, dye molecules are subject to small differences in their environment affecting the local bleach rate. We found that by fitting the fluorescence bleaching with a stretched exponential function (Eq. 2) – often used to describe polymer kinetics – that good fits with small residuals can be obtained.

$$I_f(t_b) = C + A \exp\left((-kt_b)^\beta\right) . \tag{2}$$

In Eq. 2, $I_f(t_b)$ expresses the fluorescence intensity in counts, C the non-bleaching background fluorescence intensity, A the bleached fluorescence
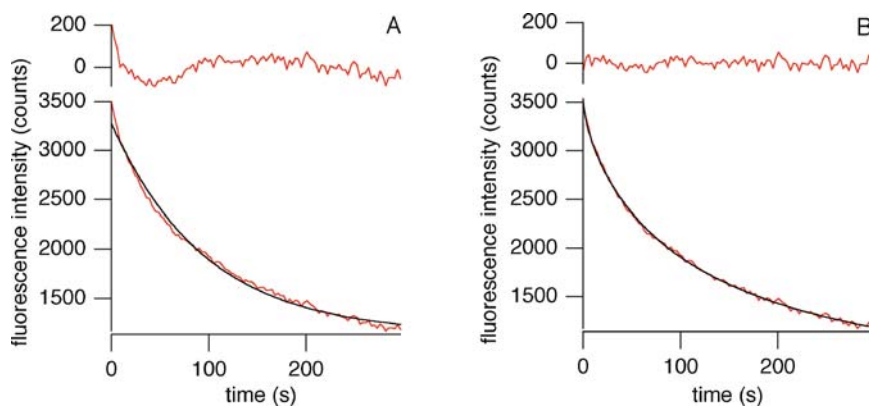
Fig. 1 Mono-exponential (**A**) and stretched exponential (**B**) fitting of the decay of fluorescence intensity measured for a single pixel with the residuals shown at the *top* of each figure

intensity, k the bleach rate, t_b the bleach exposure time, i.e., the time the layer is exposed to the illumination light and b the stretched exponential coefficient, which has a value between 0 and 1. Note that the stretched exponential function is equivalent to a mono-exponential function for $\beta = 1$. In an example on a bleach series from one pixel point, we see that the fit of the fluorescence bleaching behavior (Fig. 1) with the stretched exponential function shows a great improvement over a mono-exponential fit on the same data.

We also found (Fig. 2) that the bleach rate k obtained from the stretched exponential fitting procedure is linearly proportional to the illumination intensity within 2% over a range of excitation intensities relevant to regular arc-lamp fluorescence microscopy [1]. It is clear that such linearity is an absolute requirement for the successful application of this method for illumination calibration in practical microscopy.
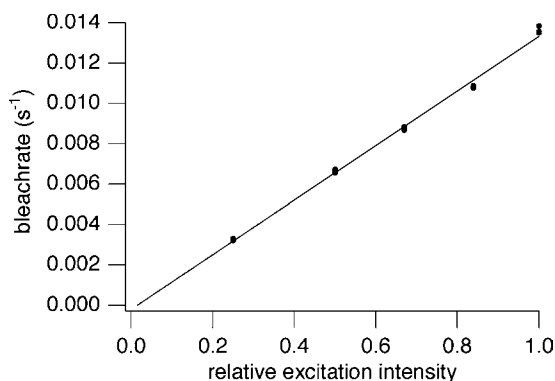

Fig. 2 Bleach rate *k* from the stretched exponential fitting procedure versus the relative excitation intensity, set by neutral density filters. 14 measurements are included

2.3
Fluorescence Reference Layer Development and Test Procedures

2.3.1
Preparation of Reference Layers

A fluorescence reference layer typically contains a fluorescent dye embedded in a uniform polymer film. For the irreversibly photo-bleaching dye we selected the well-known [7–9] highly fluorescing dye fluoresceine. It possesses suitable bleach sensitivity such that illumination calibration under typical specimen illumination conditions in an arc lamp equipped microscope can be done in a few minutes. Upon irradiation of fluoresceine in its absorption maximum, around 488 nm, an irreversible series of photo reactions takes place, leading to a change in the absorption spectrum, and therefore to a decrease in the fluorescence output, around 530 nm [7].

Since fluoresceine is water soluble, the polymer in which the fluoresceine is to be diluted has to be water soluble as well. Furthermore, the polymer solution should provide highly reproducible and well-defined layers after spinning. Polyvinylalcohols were identified as suitable polymer host layer material. Typically solutions were made comprising 0.01 wt % fluoresceine (Merck) in polyvinylalcohol (Aldrich, 87–89% hydrolyzed, MW 124 000–186 000), which were spin-coated (1250 rpm) on a 24×32 mm cover slide (Menzel), resulting in layers with a thickness – depending on the spin rate – between 150 and 200 nm and with each layer uniform in thickness within 5 nm. These layers were mounted and sealed with epoxyresin on a microscope slide (76×26 mm). Very reproducible layers could be obtained in this way. Due to the low concentration of fluoresceine we avoid intermolecular dye interactions as much as possible. As a result the fluorescence intensity from the layers is generally one order of magnitude lower then stained biological samples.

The layers are stored in the dark at room temperature and have been used more then one year after production, without any significant changes observed.

2.3.2
Instrumentation

Images were acquired with an Olympus BX60 fluorescence microscope equipped with a Photometrix Coolsnap fx digital camera. Excitation occurred with light from a Hg-arc lamp, which was filtered through an Olympus 41017-model UMF2 filter set, providing excitation at wavelengths between 451–490 nm light while transmitting fluorescence light to the camera between 491 and 540 nm. Measurements were carried out with an Olympus Ach 20x (NA = 0.4), or an Olympus UPlanFL 40x, (NA = 0.75) objective lens. Data collection and processing was done with IPLab Spectrum software from

the Signal Analys Corporation with a custom written kernel added for the stretched exponential data fits. Spin coating of the layers was performed with a Delta 10TT system from BLE Laboratory Equipment.

2.3.3
Shading Correction and Microscope Calibration Procedure

An image in a fluorescence microscope ($P(x,y)$) can be described – see Sect. 2.1 – by:

$$P(x,y) = I(x,y) \cdot D(x,y) \cdot F(x,y) \cdot t_i(s) \,. \tag{3}$$

For characterization of the microscope imaging conditions we use an image $P_r(x,y)$ of the reference layer taken under identical imaging conditions as the fluorescence image to be calibrated:

$$P_r(x,y) = I(x,y) \cdot D(x,y) \cdot F_r(x,y) \cdot t_{ir}(s) \,. \tag{4}$$

By taking the ratio of both images a calibrated image $P_c(x,y)$ is obtained:

$$P_c(x,y) = \frac{P(x,y)}{P_r(x,y)} = \frac{F(x,y)}{F_r} \cdot \frac{t_i(s)}{t_{ir}(s)} \,, \tag{5}$$

where the pixel by pixel fluorescence is normalized in units of fluorescence with respect to the reference layer. We see that the actual imaging conditions described by $I(x,y) \cdot D(x,y)$ have dropped out. The fluorescence generation is assumed to be linear with respect to illumination intensity, i.e., only dose – $I(x,y) \cdot t_i$ (s) – dependent.

With the actual pixel by pixel imaging conditions removed in this image due to the division, the calibrated image $P_c(x,y)$ directly represents a shading corrected image.

For the same reason we have seen that fluorescence images taken under different imaging conditions, if no other factors play a role, can be directly quantitatively related to each other, as they are expressed in units of the standardized fluorescence of the reference layer.

2.3.4
Separation of I(x,y) and D(x,y)

As the reference layers – as shown below – possess highly spatially uniform bleaching characteristics it is in addition possible to obtain the specimen illumination distribution $I(x,y)$ independently of the detection distribution $D(x,y)$. This illumination distribution can be derived from the analysis of the bleaching behavior of the calibration layer. For this a time series of images is taken of the reference layer during which the layer is bleached down to about 30% of its starting fluorescence intensity. Using the stretched exponential bleach kinetics described in Sect. 1 we fit the bleach decay at each pixel
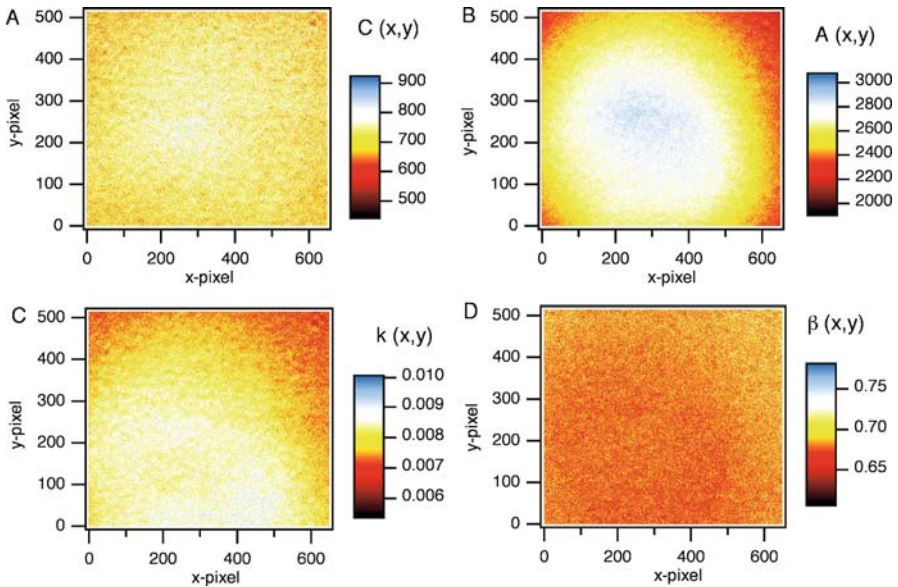
Fig. 3 Analysis of the fluorescence bleaching of a spatially uniform test layer by fitting (pixel by pixel) with a stretched exponential function. $I_f(t_b) = C + A \exp((- kt_b)^\beta)$: **A** C(x,y), **B** A(x,y), **C** k(x,y) and **D** β(x,y)

of this series of images with a stretched exponential (Eq. 2). The result of this operation can be represented as 4 images corresponding to the respective fitting parameters. A typical result obtained on our reference layers is shown in Fig. 3 with panel A the non-bleaching part of the fluorescence of the image C(x,y), panel B the bleached fluorescence intensity A(x,y), panel C the bleach rate k(x,y) and panel D the stretched exponential coefficient β(x,y). With k(x,y) = k_0·I(x,y) over the relevant range of illumination intensities (Fig. 2) the illumination intensity distribution (I(x,y) can now be derived from the bleach rate image k(x,y) apart from a constant factor. k_0 is a bleach constant for the used bleaching material. Such an illumination distribution I(x,y) can
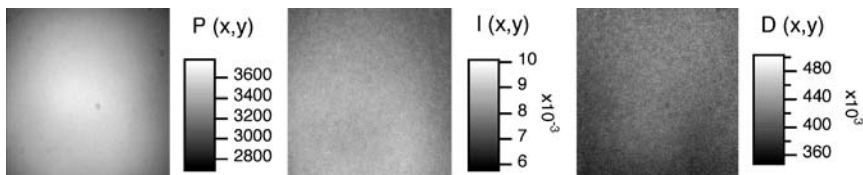

Fig. 4 The product distribution P(x,y) of the microscope (determined from the image at $t = 0$ of the test layer), divided by its illumination distribution I(x,y) (determined by the bleachrates k of the test layer), gives the detection sensitivity distribution D(x,y) of the microscope

be useful for determining the actual illumination conditions – such as alignment or uneven illumination in a microscope.

Dividing $P_r(x,y)$ by $I(x,y)$ obtained from the bleach procedure gives the detection sensitivity distribution, $D(x,y)$, of the microscope as is directly clear from Eq. 4. Figure 4 shows the results of the separation of $P(x,y)$ into $D(x,y)$ and $I(x,y)$. A remarkable feature in the $D(x,y)$ image is the appearance of dark spots solely in the detection distribution, which are due to irregularities such as dust particles in the detection pathway.

2.4
Calibration Layer Reproducibility and Uniformity

2.4.1
Uniformity of the Calibration Layer

2.4.1.1
Fluorescence

For application of the calibration procedures uniformity of the fluorescence and bleach properties across the layer are crucial. To determine if the reference layer is really spatially uniform, two fluorescence intensity images were taken at $t_b = 0$ at different spots on one reference layer (see Fig. 5g). To obtain such images, the layer is put into focus first using the diaphragm of the microscope, after which the layer is moved slightly with the light switched off. The measurement is started when the light is switched on.

The first image was then used as reference image P_r ($t_b = 0$) – Fig. 5a – and the second – Fig. 5b – as the object image $P(t_b = 0)$. Then in the test for the layer uniformity the object image was "calibrated" by dividing it by the reference image resulting in the calibrated image Fig. 5c. If now both areas imaged are both uniform and show equal fluorescence, then in the histogram of pixel values of this calibrated image, we should see a narrow distribution with an average value of 1.

This "self" test using the reference layer itself is very effective because if the layer properties would not be uniform over the image area or would differ from location to location over the layer, then such differences would immediately show up as a broadening in the calibrated image histogram.

The images shown in Fig. 5 are in fact also an excellent illustration of the effectiveness of shading correction. The "uncalibrated or raw" reference layer images $P_r(t_b = 0$ and $P(t_b = 0)$ show in their respective histograms Fig. 5d (avg. 2210; fwhm 277) and Fig. 5e (avg. 2206; fwhm 292) intensity variations of up to 29% and relative standard deviation of ca. 5%. Correction leads to Fig. 5c with its corresponding histogram (Fig. 5f) (avg. 0.999; fwhm 0.038) with a clearly improved relative standard deviation of 1.5%. Furthermore the average value of the corrected image is close to 1.0, which is the value expected for a layer with identical fluorescence as its reference.
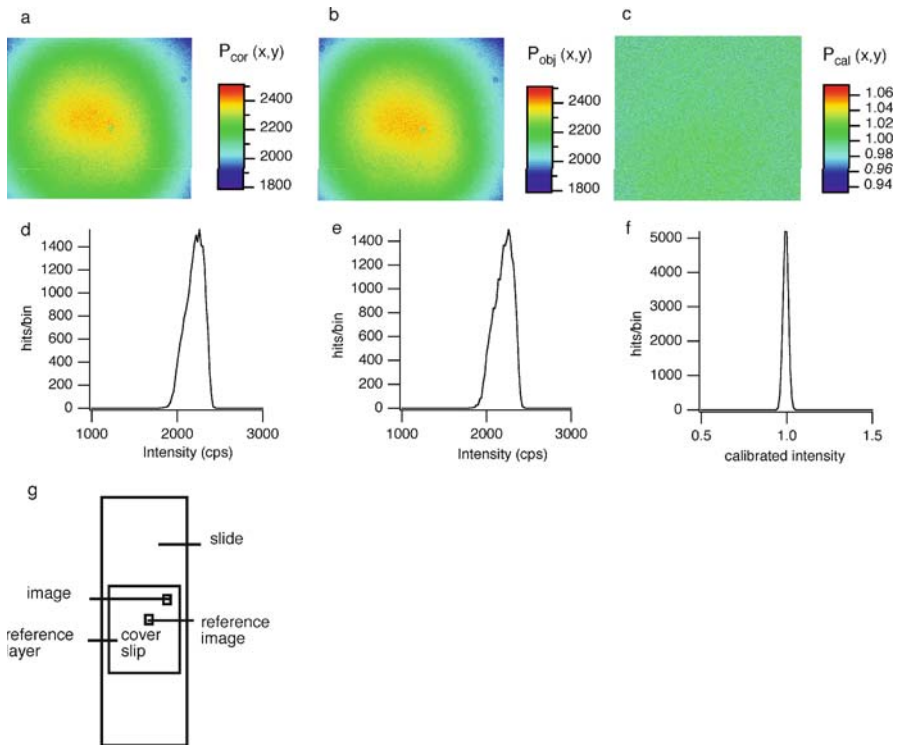
Fig. 5 The reference image (**a**) and object image (**b**) as used in the "self" test for layer uniformity with (**c**) the resulting calibrated image. **d,e** and **f** are the corresponding histograms of pixel intensity values of these images. **g** shows the configuration of the reference layer. See further text

2.4.1.2
Uniformity of Bleaching Characteristics

In a similar way as described above using the layer itself, the uniformity of the bleaching properties of the layer can be tested. The approach is correcting for the observed bleach rates in one location with the help of the illumination distribution data obtained at a second location of the layer. A narrow distribution in the bleachrate histogram in the illumination corrected bleachrate image then indicates that the bleach characteristics are indeed uniform over the layer.

A series of 100 images (515×630 pixels) was taken at identical time intervals of a reference layer. From these images an illumination distribution, $I_{cor}(x,y)$ (Fig. 6a) can be calculated as described in Sect. 2.3.4. This illumination distribution I_{cor} can now be divided by another illumination distribution, I_{obj} (Fig. 6b) obtained in a similar way at a different spot on the same reference layer or another reference layer. This results in a calibrated illumination distribution, I_{cal} (Fig. 6c).

Figure 6d–f show the histograms for the 3 images shown in Fig. 6a–c. I_{cal} is centered on 1.012 ± 0.023 (fwhm 0.054), whereas for a perfectly uniform test layer this value is expected to be one. The relative standard deviation of the uncorrected bleach rates from I_{obj} of 10.7%, after calibration is reduced to 2.3%.
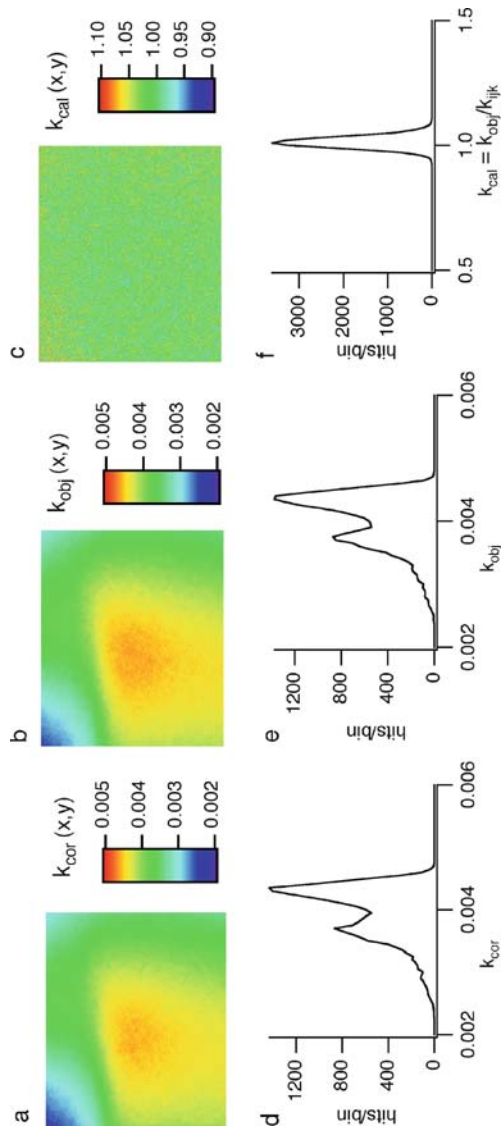

Fig. 6 Uniformity of reference layer bleach characteristics. **a** shows illumination distribution with which the bleach rate image (**b**) is corrected to obtain the uniform corrected bleachrate image (**c**). **d,e** and **f** are the corresponding histograms. See further text

2.4.2
Reproducibility of the Reference Layers

For a reference layer to be of practical use its properties should be reproducible from batch to batch during manufacturing. For a number of reference layers, prepared and measured under the same circumstances, the intensity at the onset of illumination and their respective bleach rate distribution have been measured. The results from the layers in one batch – prepared from the same fluorescer solution and under identical spinning and sealing conditions – are shown in Fig. 7A. For five samples, i.e., Fig. 7A(a–e), bleach rates with a relative standard deviation of 1.3% have been established, whereas their intensities at $t_b = 0$ have a relative standard deviation of 2.2%.

From batch to batch we observed very similar bleach properties in all properly sealed layers examined. Some variation in the absolute fluorescence intensities of the layers was observed both between batches and layers from

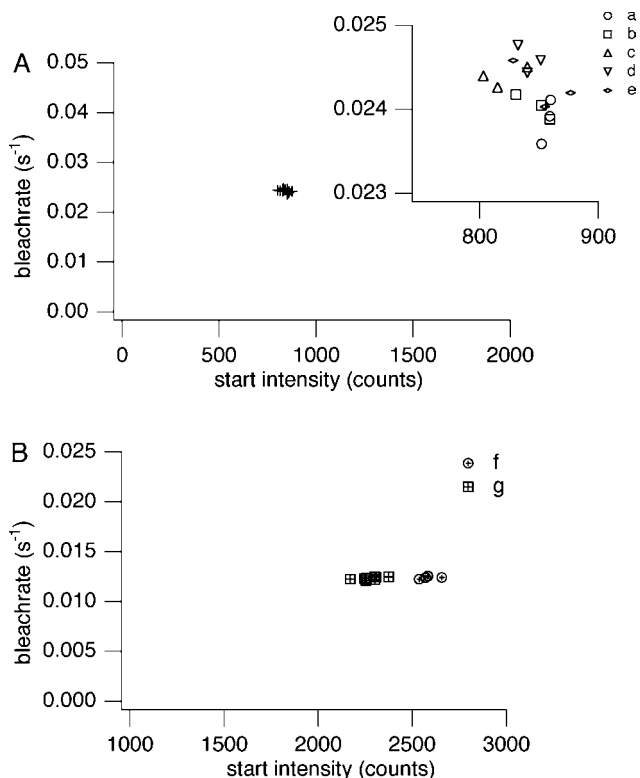**Fig. 7 A** Bleach rate versus start intensity (emission at $t_b = 0$) at different locations in one test layer, inset enlargement of measurements *a*, *b*, *c*, *d* and *e*. **B** Bleach rate versus start intensity in layers from two different batches as indicated by *f* and *g*

one batch (Fig. 7B). The relative small variation in fluorescence observed is probably caused by fluorescer concentration variations from batch to batch and – within a batch – small variations in layer thickness due to spinning conditions. Some further optimization and calibration of the layer fluorescence against a common standard or in absolute terms – see below – can address this problem.

2.5
Application Examples in Wide Field Microscopy

2.5.1
Fluorescence Intensity

2.5.1.1
Shading Correction

In addition to the result presented in Sect. 2.4.1.1 we demonstrate the effectiveness of the shading correction procedure on a sample, which has an evenly distributed fluorophore concentration associated with recognizable morphological features. For this test liquid lipid monolayers of DPPC doped with the fluorophore NBDPC on a glass substrate were prepared. These monolayers give rise to two distinct morphological features: a liquid condensed
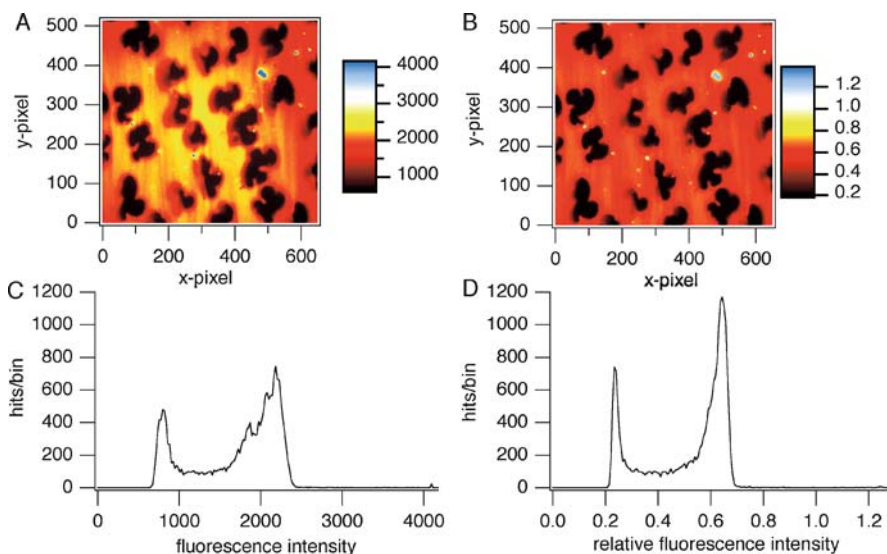

Fig. 8 False color fluorescence intensity images (**A,B**) and histograms (**C,D**) of DPPC monolayers doped with 4.4 mol % NBDPC, as obtained before (**A,C**) and after (**B,D**) shading correction

(LC) phase with low fluorescence intensity and a liquid expanded (LE) phase, characterized by higher fluorescence intensity [10, 11]. The uncorrected fluorescence image of these monolayers is shown in Fig. 8A while after correction with the reference layer image Fig. 8B is obtained. We observe after correction a much clearer association between respective regions of lower and higher fluorescence intensity and regions with LC and LE phases. The effect is also demonstrated in the histograms Figs. 8C and d of these images, where the distributions of associated with the LE and the LC phases are significantly better defined after shading correction than before.

2.5.1.2
Calibration of Microscope Conditions

It would be very valuable in fluorescence microscopy to be able to compare quantitative images taken at various imaging conditions. This is especially important as reproducing imaging conditions between microscopes – or even maintaining identical conditions in the same microscope over time – is difficult, if not impossible. When evaluating the possibilities of image calibration for comparing microscope conditions we found it to work well when comparing images obtained under similar NA conditions or different NA and similar object structure but not when both factors were different. A factor in this may be that the complexity of object structures – a flat layer vs. for instance cells of finite thickness in culture – affects the angles over which light is scattered. This may make the efficiency of fluorescence light collection NA dependent.

For the present we found it is useful to distinguish three different cases for evaluating the possibilities of image calibration as a function of microscope imaging condition:

(a) Comparing the imaging of objects in the imaging field with similar scattering properties and observed under different NA and magnification conditions.
(b) Idem with differently scattering objects but with identical NA and magnification and varying illumination conditions.
(c) Idem but with both differently scattering objects and different NA and magnification.

For demonstrating image calibration under uniform scattering we looked at images at different NA and magnification of liquid expanded and condensed lipid layers used above – see Sect. 2.5.1.1. These layers are basically flat and can be assumed to possess similar scattering properties over the whole image. We compared images obtained under $20\times$ and $40\times$ magnification. In order to compare images with these different magnifications a window which is about 1/4 of the total image in the $20\times$ image was chosen, which exactly corresponds to the area covered by the $40\times$ image. In Fig. 9 we see that
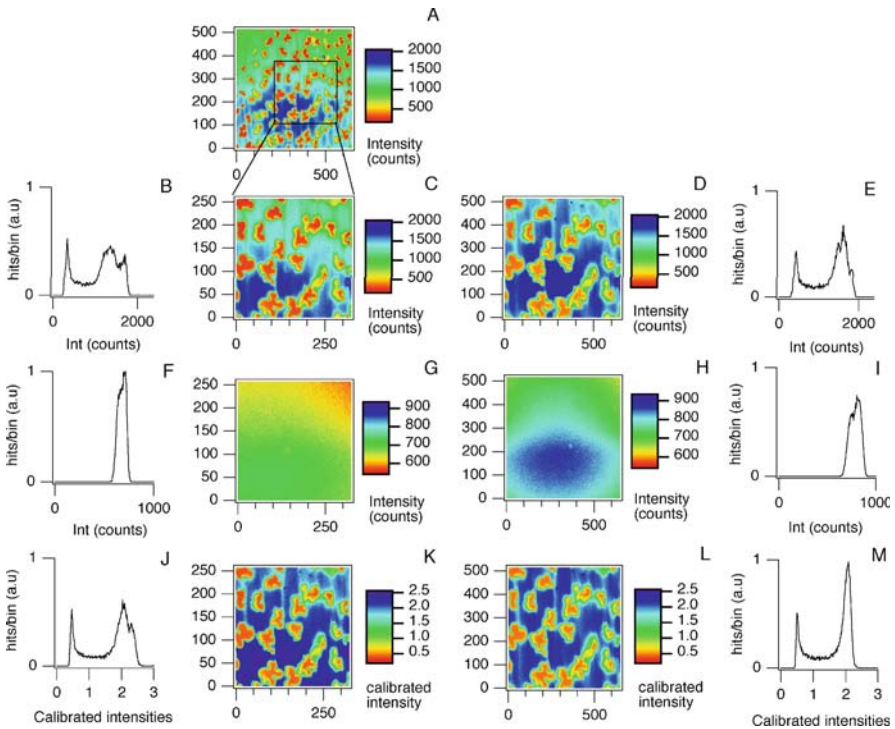
Fig. 9 Image calibration of fluorescence images of the labeled DPPC layer taken with 20×, N.A. = 0.40 (**A,C**) and 40×, NA = 0.75 (**D**) objectives respectively. For clarity the corresponding histograms are also given. Of the 20× image (**A**) the corresponding area viewed by the 40× lens (**C**) is shown as indicated by the sketch. With **C**, (**B**, histogram of **C**) and **D** (hist: **E**) serving as object images to be calibrated and **G** (hist: **F**) and **G** (hist: **H**) as reference images the calibrated 20× image **K** (hist: **J**) and 40× image **K** (hist: **L**) are obtained. From their false color representation it can be seen that the calibrated 20 and 40× images not only are shading corrected but also show closely similar calibrated intensities

the different intensity distributions in Fig. 9C and d after calibration (with Figs. 9G and H respectively) – Figs. 9K and L – show a nice correspondence and are also both shading corrected in the process.

Figure 10 shows the results of image calibration of images taken under strongly different illumination conditions, however at the same NA and magnification. These specimens are C3617 mouse cells transfected with GFP-GR (Glucocorticoid Receptor) [12]. Noteworthy is that in the ratio image h of the corrected images the non-bleaching background can be seen to have ratio values around 1 indicating good correlation between images after calibration. Due to some bleaching of the cells between the two images – image with objective 1 taken first – we see that in the ratio image h the cells show up somewhat brighter. The present result shows that in an object with some scattering and with very different product distributions – created here by on
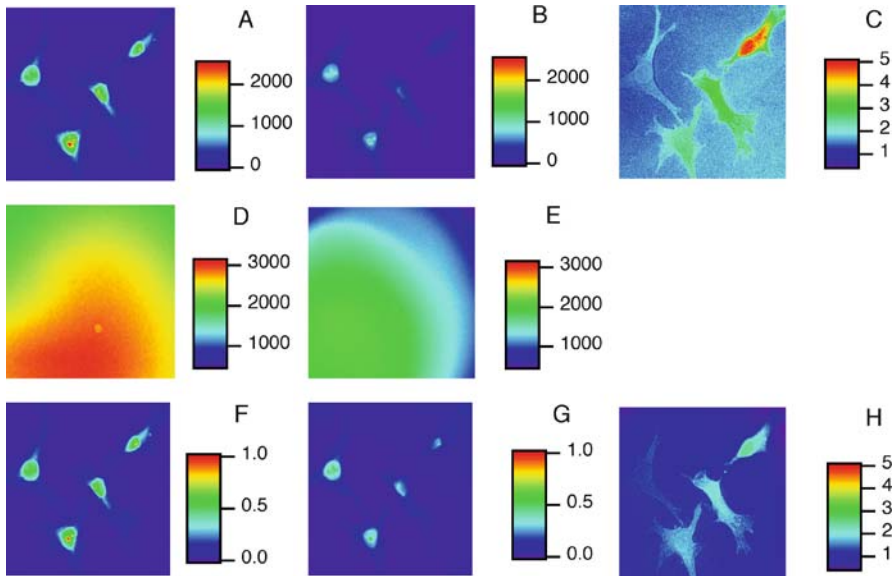
Fig. 10 Comparison imaging of C3617-mouse cells transfected with the GFP-glucocorticoid receptor using two different – but with the same NA – objectives, objective 1 and 2, and under different imaging or product distributions $P_1(x,y)$ and $P_2(x,y)$, respectively. **A** image taken with objective 1 and $P_1(x,y)$, **B** with objective 2, $P_2(x,y)$. The ratio image (**C**) (= a/b) shows very poor correlation between (**A**) and (**B**). After calibrating both images (**A**) and (**B**) with the respective product distributions **D** ($P_1(x,y)$) and **E** ($P_2(x,y)$) we see that the corrected images, **F** and **G** respectively, show much better correlation as also witnessed by the ratio image (**H**) (= f/g)

purpose disaligning the illumination conditions between the objective 1 and 2 images – still good image correlation can be achieved.

We found in preliminary experiments that on objects with finite scattering such as the cells used above, and observed under different NA and magnification conditions differences of up to 20 to 30% could be observed between the calibrated fluorescence of these objects, differences which could not be explained by bleaching. As indicated above these differences after calibration may be tentatively associated with the varying scattering properties of the structures imaged. A systematic exploration of this subject has not been done yet but we hope to address this issue at a later time.

2.5.2
Bleach Rate Imaging and Correction for Uneven Illumination

Bleach rate imaging becomes practical if the effect of uneven illumination – producing uneven bleaching over the image – can be corrected. We found during the imaging of the NBD chromophores present in the monolayers as
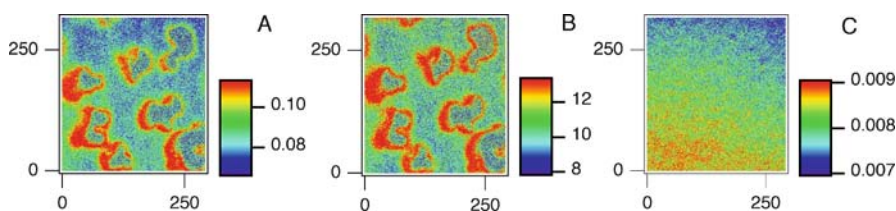
Fig. 11 False color images of the bleaching constants before (**A**) and after (**B**) illumination correction measured for DPPC monolayers doped with 4.4 mol % DPPC-NBD. **C** shows the illumination distribution used during the correction

described in Sect. 2.5.1.1, Fig. 8 that these are subject to substantial bleaching. Figure 11a shows the bleach constant k(x,y) image obtained by fitting with the stretched exponential fitting procedure an image bleach series of the central area shown in Fig. 8 corresponding to about 1/4 of the original image. After correction with the illumination distribution – Fig. 11C – we see in the corrected image Fig. 11B that both the LE and the LC phases bleach at a similar rate. However, in the phase coexistence region, the monolayer bleaches about 25% faster. While the underlying reason for this behavior is not fully clear – it could be associated with reduced ordering in the phase coexistence region – this result still shows that imaging in the bleach constant parameter can indicate new features in the image which would remain unnoticed otherwise.

3
Characterization of Sectioning Fluorescence Microscopy (3D) with Thin Uniform Fluorescent Layers: Sectioned Imaging Property or SIPcharts

3.1
Introducing Calibration in Sectioned Fluorescence Microscopy

Three-dimensional fluorescence microscopy has found widespread application in recent years, especially in molecular cell biology. Imaging in this type of microscopy is usually based on a series of sectioned images obtained by stepping the specimen through the focal region of a beam type scanning microscope. In most confocal or two-photon microscopes the signal at each lateral image position in a section is digitized and the data subsequently stored – together with the data of the other sections – as a 3D dataset. Ideally, the imaging properties should be identical over the imaging field. However, already at the inception of confocal microscopy it was realized that for instance the apparent fluorescent intensity in confocal imaging could vary significantly over the image field [13]. Also the actual confocal imaging conditions do vary

significantly from microscope to microscope. In fact the actual sectioning properties of an instrument and the apparent image intensities are observed to depend sensitively on its optical properties related to the optics employed, and operator controlled factors like pinhole and alignment settings. The latter two factors especially cause uncertainty in reproducing settings with confidence making the comparison difficult of images obtained during different confocal sessions.

Up till now to our knowledge no reasonably easy to use and effective means are available for describing a particular imaging situation in 3D microscopy. Here we propose the use of thin uniformly fluorescing layers for characterizing the confocal or more general sectioning properties of a particular imaging situation. It has the specific advantages that it gives a good "feel" for the sectioning properties over the image field, is sensitive to small changes in the imaging conditions and possesses good signal to noise properties under regular imaging conditions, the latter because the fluorescence data from the thin layers can be binned to a substantial degree without loss of information on the lateral variation of measured sectioned imaging characteristics properties (see below). Its ease of use makes it feasible to use this method for routine determination and analysis of the 3D imaging properties as a function of parameters such as pinhole settings, alignment, and other parameters.

The method is based on the uniform fluorescent reference layers as utilized above for the calibration of regular wide-field fluorescence microscopy. Their uniform thickness and uniform fluorescence properties are also essential for the success of the presented method for 3D calibration. Schrader et al. [14] employed very thin – order of nms – fluorescent layers for monitoring the resolution in 4pi-microscopy. Their layers were neither aimed for use for general characterization of sectioning microscopy, nor specifically developed and tested for lateral uniformity.

3D datasets acquired by the deconvolution of non-scanned regular fluorescence images [15] can also, in principle, be characterized by the present approach: applications are restricted here to sectioned imaging obtained by the scanning approach.

It is to be noted that in the present approach only access is obtained to the axial imaging characteristics (or axial PSF, see below) but *not* the lateral variation of the point spread function (PSF) governing the imaging. While this constitutes a limitation on the presented method, we think that the axial PSF gives at least an excellent indication of the quality of a particular sectioned imaging system. Often the results will be more then sufficient for judging the relative imaging conditions between sessions or instruments with the ease of use and sensitivity of the method outweighing this limitation.

In Sect. 3.2, some basic aspects of confocal and 2-photon sectioned imaging by the scanning approach are described as an aid to the understanding of the sectioning imaging effects characterized by the presented method.

3.2
Imaging in Confocal and Two-Photon Scanning Microscopy

The image formation in confocal microscopy is governed by the confocal point spread function (PSF) formed by the product of the illumination distribution and detection sensitivity function distributions overlapping in specimen space. The former is given by the spatial distribution of the focused laser illumination while the latter refers to the spatial distribution of the probability that the fluorescence photons generated in the specimen by the focused laser excitation will in fact be detected and contribute to the imaging. Optically this distribution is represented by the back projection of the detection pinhole into specimen space.

Optimally the confocal PSF should be the product of ideal or diffraction limited illumination and detection distribution functions perfectly overlapping over the whole of the lateral imaging field both in the center as well as at the borders of the imaging field.

However, optical aberrations or alignment errors and often a combination of both may prevent this from being the case. For instance chromatic aberration in combination with off-axis aberration can cause relative walk-off of distributions, which were adjusted during alignment for optimal overlap in the center of the scanned image field. (Fig. 12). This then will result in a re-
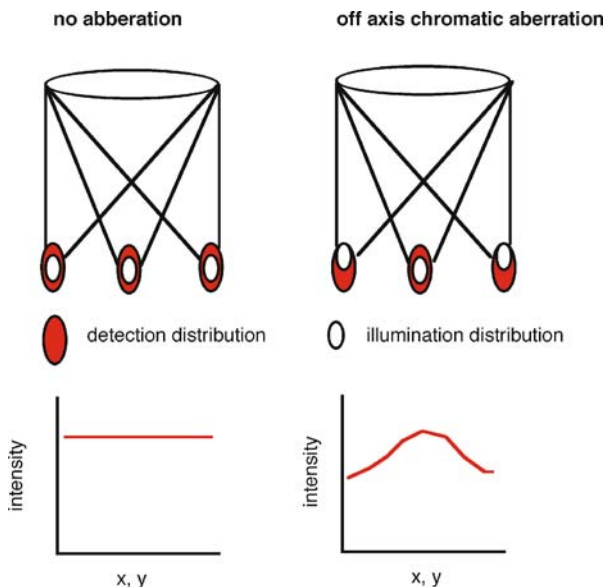
Fig. 12 Conceptual illustration of the walk-off due to chromatic aberration at off-axis scan-field positions between illumination and detection distributions and the resulting reduction in the detected confocal signal

duced confocal signal in the off-center regions. Also other parameters like the axial resolution may be similarly affected and often – see below – in an irregular manner over the imaging field.

In multi-photon microscopy the fluorescence generation in the specimen is proportional to the quadratic or higher power of the intensity of the focused excitation radiation in the microscope. Well focused, diffraction limited excitation distributions result in the highest multi-photon yield. This makes the fluorescence generation in this type of imaging sensitive to various on-axis and off-axis aberrations in the focusing of the excitation radiation during the scanned acquisition of a multi-photon image. As mostly no detection pinhole is employed, the situation on the signal collection side will be less critical.

A more extended treatment of both types of imaging has been written by Diaspro [16].

3.3
Sectioned Image Characterization, Principle and Analysis Parameters

3.3.1
Principle of the Method and Definition of the Axial PSF

The presented sectioned imaging characterization method utilizes a 3D image or data stack of a thin uniform fluorescence or reference layer, acquired through the standard 3D imaging routines as available in most confocal or two-photon microscopes. When the fluorescent reference layer is stepped through the confocal region in this routine the fluorescence signal at each lateral image point will track the axial dependence of the *laterally* integrated intensity of the confocal PSF, or "axial PSF," as further explained in Fig. 13.

It is essential in order to be able to measure the axial variations of the axial imaging properties with acceptable resolution that the layers used are reasonably thin with respect of to the dimensions of the axial point spread function. On the other hand a "too thin" layer will lead to lower signal to noise in the fluorescence data. With a typical axial PSF width under high NA conditions of around 700 nm we found that a layer thickness of the order of 100 nm proved a good compromise. The measured axial PSF will be in fact a convolution of the actual PSF. The increase in the apparent width due to the convolution of a layer of finite thickness will be approximately by a factor of $\sqrt{(1 - (l/w)^2}$ with l the layer thickness and w the axial width of the PSF [17].

Similarly as wide field applications we have found that the fluorescent layers need to be laterally uniform to a high degree. Only then will the axial responses found at each x-y point do indeed represent a correct measurement of the axial PSF suitable for establishing the sectioned imaging characteristics at the various lateral points of the sectioned image. The layers, with a thick-
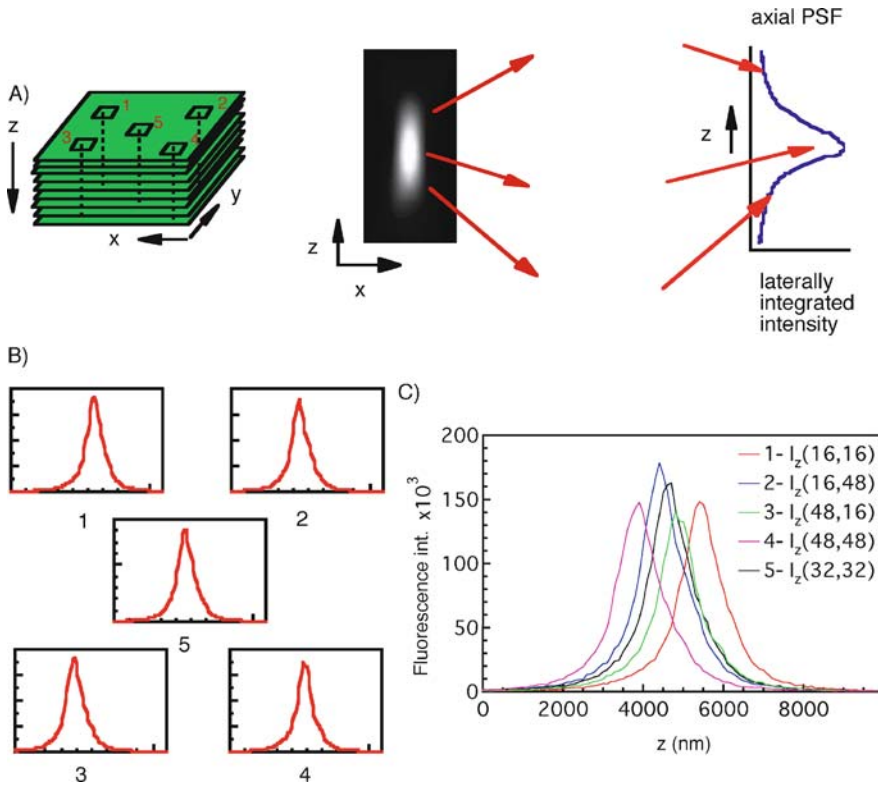
Fig. 13 The 3D image characterization is based on a 3D-data stack acquired by stepping a thin uniform fluorescence reference layer axially – i.e., along the z-axis – through the confocal region. As illustrated in (**A**) the set of values found at a particular x-y position as a function of z in the stack represent the axial variation of the laterally integrated PSF as sampled by the thin – about 100 nm – fluorescence reference layer. This set of values is called the axial PSF, the shape and amplitude of which will track the variations of the underlying PSF over the image scan field, as illustrated for field positions 1 to 5 in (**B**) and collected together in (**C**)

ness of ca 100 nm used for this application satisfy this condition with their fluorescence intensity and layer thickness uniformity similar to the ones described before [18]. With the layers sufficiently thin and uniform, the axial or z dependence of the fluorescence at each lateral image point in the 3D dataset of such a layer will in fact represent the axial PSF and can thus be used for characterizing the sectioned imaging at that point. Figure 13b and c show, as an example, taken from an actual measurement, the axial responses measured at 5 locations in the imaging field, showing that the actual axial PSF does vary over the imaging field. This is not unexpected in a beam scanning confocal instrument where the axial PSF may indeed be affected by off-axis optical aberrations in one form or another.

3.3.2
Analysis of the Axial PSF Properties

Various choices can be made to analyze these axial PSF responses in the terms of parameters. At present we have chosen the following, (see also Fig. 14):

I_{total} the total integrated intensity under the axial PSF response;
I_{max} the maximum fluorescence intensity found along the axial response;
Z_{max} the axial position at which the value of Imax is found;
fwhm   the axial resolution as represented by the fwhm of the axial response;
skew s   axial asymmetry of the axial PSF response.

For the purpose of this paper the skew s is defined as $s = (a - b)/(a + b)$ with a and b evaluated at the level of half maximum intensity of the axial PSF as indicated in Fig. 14. The sectioned imaging properties of a given system can conveniently be represented in a so-called sectioned imaging property chart or SIPchart (see Fig. 15a and b) based on the above parameters. As these parameters can be determined at each point in the lateral image field it is a logical step to represent the data in these charts in the form of color-coded images or maps. In addition the average and variation of the above parameters over the image can be calculated and are added as an inset in the respective color coded images. These values, summarized in a separate table, are useful for a numerical characterization of the imaging properties over the whole image field. The axial resolutions of the system, white against
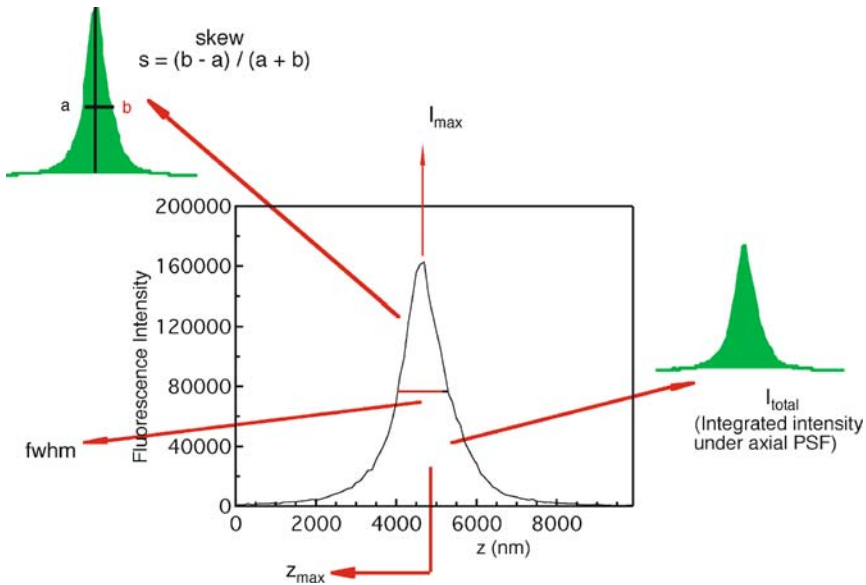

Fig. 14 Parameters for the characterization of the axial imaging characteristics of a sectioning microscope
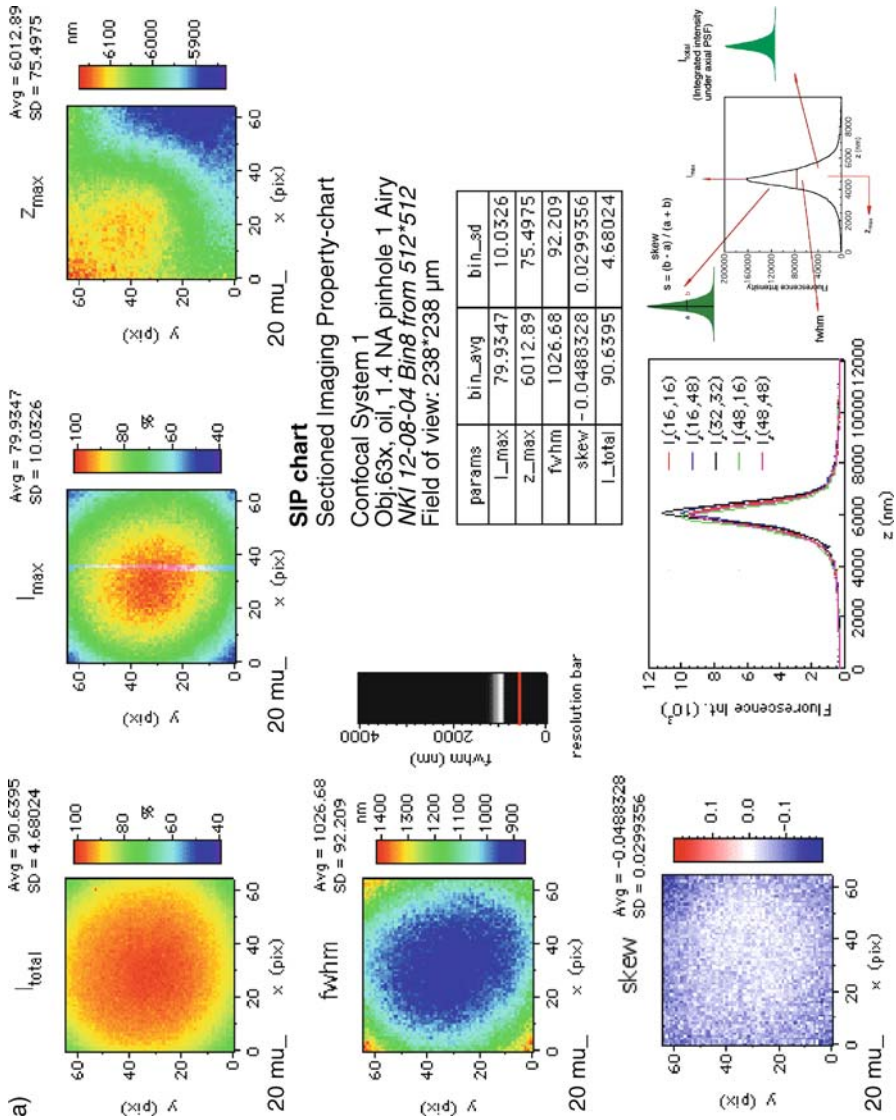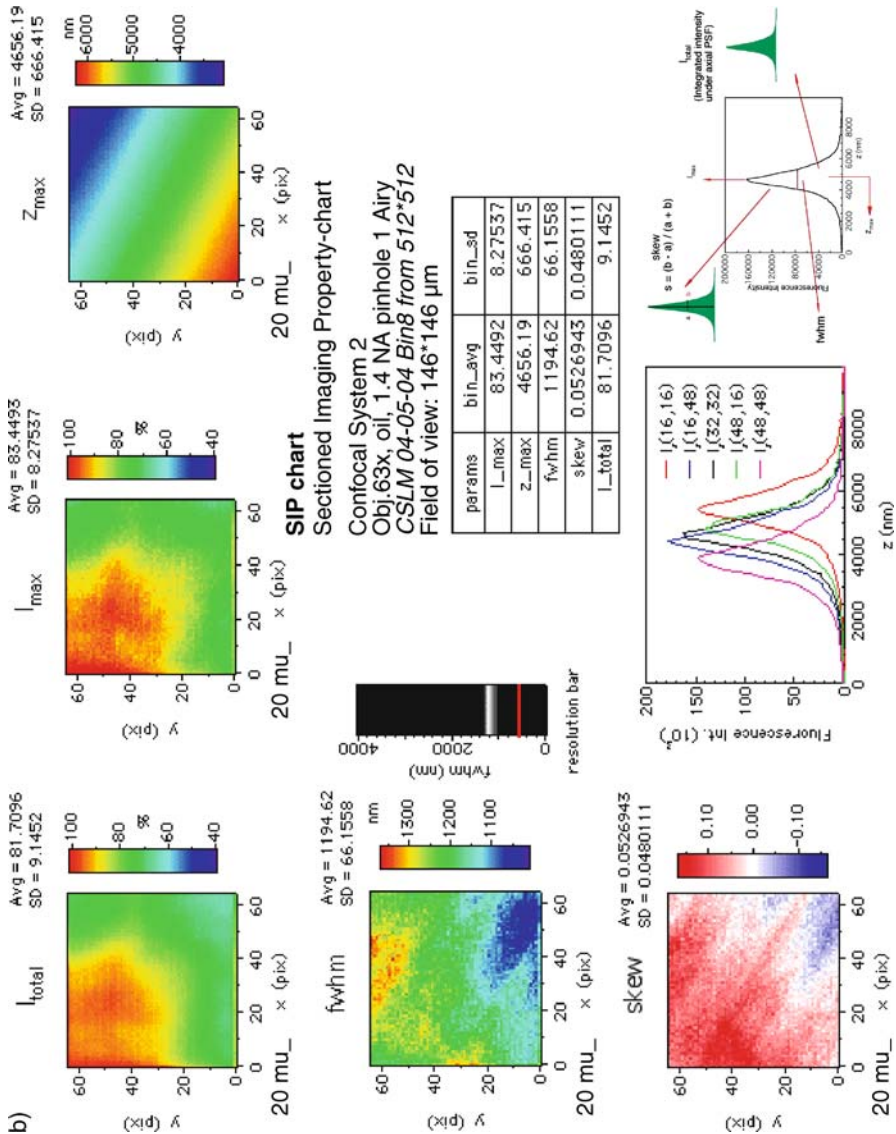
Fig. 15 (**a**) Sectioned Imaging Property charts or SIPcharts for two confocal microscope systems: SIPchart of confocal microscope system 1

the black background of the resolution bar, can be compared directly with the theoretical resolution – in red – to be expected at zero pinhole size and the numerical aperture NA of the used objective. Also included in the SIPchart are the actual axial responses measured in the center and 4 off-center locations. The SIPcharts shown are from an actual comparison of the sectioning conditions between 2 confocal systems as further discussed in the next sec-

Fig. 15 (**b**) Sectioned Imaging Property charts or SIPcharts for two confocal microscope systems: idem of confocal microscope system 2. Both microscope systems are equipped with NA 1.4, 63× oil immersion lenses and operating at the same nominal pinhole setting of 1 Airy. See further text

tion. The color coded images are binned in this case to 64 by 64 from a set of images originally of 512 by 512 image points. As the various imaging properties can be assumed – and are in fact observed – to vary relatively slowly over the imaging field, this binning while improving signal to noise conditions

does not cause any significant loss of information on the lateral variation of the represented parameters.

3.4
SIPcharts and 3D Imaging Assessment

The utility of SIPcharts for 3D image characterization is illustrated with an example based on SIPcharts taken from a comparison of two different confocal microscope systems <u>1</u> and <u>2</u> as presented in Fig. 15a and b, respectively. It should be noted that the point of this discussion is not to determine if one of the microscope systems is superior to the other, but to show that SIPcharts can be effective for evaluating and comparing their relative imaging properties. Both systems 1 and 2 are equipped with similar oil immersion lenses ($63\times$, NA 1.4) and examined under similar settings for nominal pinhole (1 Airy) and zoom. For each measurement a 100 step z-scan with was made through focus. In both cases a zoom is chosen such that a – for this objective extended – scan field resulted: 238×238 μm for system 1, and 146×146 μm for system 2.

The panels I_{total} represent the integrated intensity along the axial response over the field and permit one to judge – together with the panels I_{max} – the degree to which the apparent fluorescent intensities in the confocal images are affected by not-optimal sectioned imaging. The I_{max} panel is useful to judge the maximum difference in apparent fluorescence in the separate sections due to microscope factors while integrated I_{total} panel has a similar function for extended depth or axially integrated images. With fluorescer distribution in the reference layers to a high degree laterally uniform, one would expect under ideal imaging conditions that the both the integrated I_{total} and the I_{max} images to show uniform fluorescence over the image field. That this is not the case is clear from a first glance at these panels. Looking in more detail it can be seen that the Imax panels of the SIPcharts of both systems show a variation in the maximum fluorescence intensity of 20% and 30%. For system 1 we see a maximum located around the center of the image field with the intensities falling off smoothly towards the edges. For system 2 a much more disordered, non-symmetrical, distribution over the image field of the axial PSF maxima is observed.

The Zmax panels show the axial positions at which the maxima shown in the Imax panels were found. In both cases we see that these are located in an approximately flat plane; however, these planes are not fully perpendicular to the optical axis but somewhat tilted by 300 nm (system 1) and 2600 nm (system 2), respectively, over the image field. The possible cause of these small tilts (up to 2% for system 2 over the image field) may be either a tilt of the specimen table with respect to the optical axis or an artifact connected to the optical scanning technique used.

Assuming that the observed fwhm values of the axial responses are close to and representative of the axial resolution then from the fwhm panels a good

impression can be obtained of the resolution variations over the image field. We see that for system 1 areas with higher resolution correspond well with those with maximum intensities (I_{max}), as can be expected for a reasonable aberration free system. For system 2 this correspondence is not so clear-cut. In fact, the fwhm panel resembles the skew panel better then the Imax panel does. This suggests that aberrations in the latter system play an appreciable role in the image formation, as also witnessed by the much greater values for the skew and skew variation observed there. Also, comparing both systems, it is interesting to note that while in system 1 the average resolution is somewhat better than system 2, the opposite is the case for the resolution variations over the field. Thus system 2 has a more uniform resolution over the image field. The same is also the case for the fluorescence intensity variation as can be seen from the lower standard deviation of the Imax values for system 2. Of course, when making this judgement it should be noted that the imaging field shown of system 2 is appreciably smaller then the one of system 1.

The skew parameter s as defined in Fig. 14 is a parameter characterizing the first order asymmetry of the axial PSF and may be indicative of the presence of spherical or other optical aberrations. The severity or degree of aberration can and indeed often does vary over the image field. Comparing the data in the skew panels of the SIPgraphs of both systems very low skew values are seen close to 0 in the case of system 1 while in for system 2 a more irregular, somewhat striped pattern is seen with local skew values varying from 0.15 to –0.15.

The black resolution bar is useful to get an "at a glance" impression of the axial resolution and resolution variations of the system – the white band – in relation to the theoretically possible resolution – the red bar – at zero pinhole size. Finally in the SIPcharts the actual axial responses are given at 5 locations in the image field. With a binned image size of 64 by 64 the curve Iz(16,16) represents the axial response taken at point $x = 16$ and $y = 16$ etc. The availability – in the lower, middle panel of the SIPchart – of the actual responses is useful to recognize the presence of strong aberrations which sometimes cannot be effectively recognized from the fwhm and skew parameters values only.

System 1 and 2 represent two systems of major confocal manufacturers which were evaluated by the SIPchart method in the state we found them, including for instance, sub-optimal user alignment, etc. It is neither proper nor relevant for the purposes of this paper to further identify these systems, as the presented data are not necessarily representative of the imaging attainable with the instruments.

3.5
SIP-Charts, Analysis Examples, and Sensitivity

SIPcharts present a great amount of data to the researcher, which can serve subsequently as a convenient starting point for analysis of specific aspects of

the imaging. SIPcharts and data extracted from them are effective and convenient tools for analyzing sectioned imaging conditions and are sensitive enough for tracking differences or changes in sectioned imaging conditions. Using the SIPcharts, various specific imaging aspects can easily be compared by directly extracting the applicable data/images from the SIPchart document for documenting the sectioning conditions under which, for instance, confocal images were acquired.

While for further examples of the use of SIPcharts in sectioning microscopy we refer to Brakenhoff et al. [19] we would like to include here one application illustrating the use of SIPcharts for tracking the influence of spectral conditions on sectioned imaging. Modern confocal microscopes can collect simultaneously or sequentially images at different excitation and detection wavelength settings. However, it is well known that image plane-shifts and other effects between imaging conditions may occur due to chromatic effects in the imaging. These can be documented very well with the help of the described procedures and the SIPchart representation. Figure 16A and B show the Z_{max} panels extracted from the SIPcharts of a microscope system acquired at two spectral settings: the first for excitation at 488 nm, using a detection band-pass filter of 503–530 nm and the second with a 543 nm excitation and 560–615 nm detection band-pass filter. The through-focus data stacks for both SIPcharts were obtained in one experimental run not changing the position of the reference layer (which in this case is based on a red fluorescing dye), only changing the filter settings. The full charts are shown to illustrate that many subtle differences may be noted between the imaging between both imaging conditions. Particularly important for work where data with a different spectral signature are correlated – as in the co-localization or FRET studies – is that not only the image planes between both conditions are found to be shifted with respect to each other but also that this shift is not uniform over the imaging field. Figure 16C, obtained by processing the Z_{max} data of these SIPcharts, illustrates this nicely.
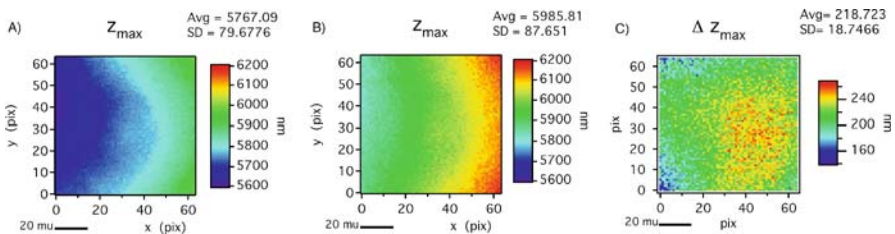

Fig. 16 Axial image plane position as a function of wavelength derived from SIPcharts of a multi-channel confocal microscope. Wavelength conditions: **A** excitation 488 nm, detection band-pass 505–530 nm, **B** excitation 543 nm, detection band-pass 560–615 nm. The data shown in panel (**A**) and (**B**) are represented on a common color scale. Panel **C** shows the axial height difference of the sectioned plane imaged at the two spectral conditions

4
Conclusions

We have shown in this chapter that using thin uniform fluorescent layers it is possible to do effective characterization and calibration in fluorescence microscopy. A major motivation behind effective calibration is that it would enable microscope users to derive quantitative specimen information from the primary fluorescence of their objects, to a first order independent of the microscope systems used. At present, quantitative data in microscopy are often determined by methods such as fluorescent life time, FRET [20] and FRAP [21], or ratiometric methods for measuring ion concentrations (Ca^{2+}, pH and others) [22].

Key to the presented approach is the availability of sufficiently uniform and reproducible layers as, for instance, produced here by spinning techniques.

The presented fluorescence reference layers may have significant value for characterizing microscope properties in general well beyond just their application in fluorescence microscopy quantification. For instance fluorescent yields under known illumination conditions allow microscope throughput or efficiency under various optical conditions to be assessed. Such illumination conditions can in fact be derived from layers with known uniform bleaching properties which were the basis of the bleach rate imaging demonstrated here. The bleach rate can serve as an environmental probe as the local bleach rate is known to be dependent on environment factors such as pH and molecular binding or as a proximity probe, the latter, for instance, through the mechanism that the mutual distance between excited molecule influences bleach probability [7, 23]. For the characterization and aligning of confocal microscopes presently different methods are employed. For instance, confocal microscopes are often aligned by maximizing the fluorescence yield from a slab of solid fluorescent material at the center of the image field. However no axial information becomes available for judging/optimizing sectioning conditions, possibly leading to sub-optimal instrument alignment. 3D imaging of fluorescent spheres can in principle give access to the full 3-dimensional point spread function, provided these beads are small in relation to the PSF. A limitation is that the small size and the hence limited number of fluophore molecules contained in these beads may make it difficult to obtain a sufficient fluorescence signal for accurate PSF determination before bleaching sets in. Also, we have found in practice that a substantial variation in apparent fluorescence between beads can be observed in many commercially available beads.

In contrast, thin uniform reference layers can provide axial PSF information at sufficiently low illumination conditions such that bleaching plays a minor role. Of course they do not provide access to the lateral PSF properties, but they do have the advantage that the laterally uniform layer fluorescence assures that fluorescence intensity variations related to instrumental properties are correctly mapped.

The SIPcharts, together with the underlying data could, in principle, be employed for correction purposes; correcting for the often observed variations in fluorescence intensity yield over the image field first comes to mind. We think the data contained in the total intensity image of the SIPchart can be used for an approximate first order correction.

Present day de-convolution algorithms are in general assuming a constant PSF over the image field. The data contained in the maps of the fwhm and skew variations in the SIPchart can be used to assess if this assumption is reasonably correct. Advanced de-convolution algorithms – incorporating PSF variations over the image field – can in principle be constructed. The presented skew and fwhm panels of the axial PSF can be a good starting point for such procedures.

Co-localization studies require accurate knowledge of relative axial positions of specimen elements imaged under different excitation and detection spectral conditions. Both on- and off- axis chromatic aberrations may cause shifts in the axial position at which these elements appear in the 3D image. By analyzing 3D datasets of the reference layer obtained at various wavelength conditions of a suitable reference layer we showed that the axial chromatic shift can be charted over the image field. We think that such shift data can be used for correction for such chromatic effects. At present lateral chromatic shifts cannot yet be tracked with the laterally uniform reference layers, but we are considering approaches to overcome this limitation.

We found – not shown here – that the presented characterization method can be very effective for the evaluation of the relative performance of otherwise identical microscope objectives when mounted on the same microscope.

The present work was mostly done using fluoresceine based uniform thin layers with an optimum excitation sensitivity around an excitation wavelength of 480 nm, but usable in a range from 430 to 490 nm. Layers suitable for any excitation and detection range are under development, with already promising results. In fact the data on chromatic effects on imaging – Fig. 16 – were acquired using a more red sensitive dye in the layer.

In this paper it is shown that the quantification and correction of fluorescence imaging can be successfully realized in wide field fluorescence imaging. Extension to sectioned microscopy imaging, a subject we are at present working on, seems to be feasible and the SIPchart representation of microscope system properties may be a good starting point for realizing this goal.

References

1. Ghauharali RI, Hofstraat JW, Brakenhoff GJ (1998) J Microsc 192:99
2. Ghauharali RI, Brakenhoff GJ (2000) J Microsc 198:88
3. Castleman KR (1979) Digital Image Processing. Prentice-Hall, Englewood Cliffs, New Jersey
4. Jericevic Z, Wiese B, Bryan J, Smith LC (1989) In: Taylor DL, Wang Y (eds) Quantitative fluorescence imaging and spectroscopy, vol B. Academic Press Inc., San Diego, California
5. Arbe A, Colmenero J, Monkenbusch M, Richter D (1998) Phys Rev Lett 81:590
6. Levitus M, Talhavini M, Negri RM, Atvars TDZ, Aramendia PF (1997) J Phys Chem B 101:7680
7. Song L, Hennink EJ, Young IT, Tanke HJ (1995) Biophys J 68:2588
8. Talhavini M, Atvars TDZ (1998) J Photochem Photobiol A 114:65
9. Talhavini M, Atvars TDZ (1999) J Photochem Photobiol A 120:141
10. Leufgen KM, Rulle H, Benninghoven A, Sieber M, Galla H-J (1996) Langmuir 12:1708
11. Kagener V, Möhwald H, Dutta P (1999) Rev Mod Phys 71:770
12. Walker D, Htun H, Hager GL (1999) Methods 19:386
13. Sandison DR, Williams RM, Wells KS, Strickler J, Webb WW (1994) In: Pawley J (ed) Handbook of confocal microscopy. Plenum Press, New York
14. Schrader M, Hofmann UG, Hell SW (1998) J Microsc 191:135
15. Agard DA, Hiraoka Y, Shaw P, Sedat JW (1989) Methods Cell Biol 30:353
16. Diaspro A (2002) Confocal and two photon microscopy. Wiley-Liss, New York
17. Bracewell R (1965) The Fourier Transform and its Applications. McGraw-Hill Book Company, New York
18. Zwier JM, Rooij GJV, Hofstraat JW, Brakenhoff GJ (2004) J Microsc 216:15
19. Brakenhoff GJ, Wurpel GWH, Jalink K, Oomen L, Brocks L, Zwier JM (2005) J Microsc 219:122
20. Jares-Erijman EA, Jovin TM (2003) Nat Biotech 21:1387
21. Sprague BL, McNally JG (2005) Cell Biol 15:84
22. Fricker M, Runions J, Moore I (2006) Annu Rev Plant Biol 57:79
23. Ha T, Xu J (2003) Phys Rev Lett 90:223002